

# A Global Survey of Lithospheric Flexure at Steep-Sided Domical Volcanoes on Venus Reveals Intermediate Elastic Thicknesses

Madison E Borrelli<sup>1</sup>, Joseph Ghilarducci O'Rourke<sup>1</sup>, Suzanne E Smrekar<sup>2</sup>, and Colby M Ostberg<sup>3</sup>

<sup>1</sup>Arizona State University

<sup>2</sup>Jet Propulsion Laboratory

<sup>3</sup>University of California

November 26, 2022

## Abstract

Topographic flexure in response to vertical loads reveals key lithospheric properties, including elastic thickness and the heat flow from the interior. Flexural stresses may also control volcano morphology. One previous study predicted that steep-sided domes on Venus usually form where the elastic thickness is  $\sim 15\text{-}40$  km. We surveyed flexural signatures around steep-sided domes and confirmed this hypothesis. We determined elastic thickness from topographic profiles with a curve-fitting algorithm and a plate bending model in Cartesian and axisymmetric geometry. We used a yield stress envelope to convert elastic thickness and plate curvature into mechanical thickness and surface heat flow. The average elastic thickness for domes not near coronae is  $\sim 30$  km, corresponding to a heat flow of  $\sim 60$  mW/m<sup>2</sup>. Coronae on Venus are typically associated with elastic thicknesses of  $<10\text{-}15$  km. Domes near coronae yielded elastic thicknesses in this range, and higher heat flows than domes not near coronae.

# **A Global Survey of Lithospheric Flexure at Steep-Sided Domical Volcanoes on Venus Reveals Intermediate Elastic Thicknesses**

**M. E. Borrelli<sup>1</sup>, J. G. O'Rourke<sup>1</sup>, S. E. Smrekar<sup>2</sup>, C. M. Ostberg<sup>3</sup>**

<sup>1</sup>Arizona State University, School of Earth and Space Exploration, Tempe, AZ.

<sup>2</sup>Jet Propulsion Laboratory, California Institute of Technology, Pasadena, CA.

<sup>3</sup>University of California, Department of Earth and Planetary Sciences, Riverside, CA.

Corresponding author: Madison Borrelli (meborrel@asu.edu)

## **Key Points:**

- We conducted the first global survey of lithospheric flexure at steep-sided domical volcanoes (pancake domes) on Venus
- Steep-sided domes on Venus are typically but not always located in regions with elastic thicknesses between ~15 and 40 km
- Domes near coronae are associated with lower elastic thicknesses and higher surface heat flows, consistent with results from prior studies

## Abstract

Topographic flexure in response to vertical loads reveals key lithospheric properties, including elastic thickness and the heat flow from the interior. Flexural stresses may also control volcano morphology. One previous study predicted that steep-sided domes on Venus usually form where the elastic thickness is  $\sim 15\text{--}40$  km. We surveyed flexural signatures around steep-sided domes and confirmed this hypothesis. We determined elastic thickness from topographic profiles with a curve-fitting algorithm and a plate bending model in Cartesian and axisymmetric geometry. We used a yield stress envelope to convert elastic thickness and plate curvature into mechanical thickness and surface heat flow. The average elastic thickness for domes not near coronae is  $\sim 30$  km, corresponding to a heat flow of  $\sim 60$  mW/m<sup>2</sup>. Coronae on Venus are typically associated with elastic thicknesses of  $<10\text{--}15$  km. Domes near coronae yielded elastic thicknesses in this range, and higher heat flows than domes not near coronae.

## Plain Language Summary

Volcano shape as seen on the surface can be used to learn about the interior of a planet. Others have hypothesized that steep-sided dome volcanoes (also called pancake domes) on Venus likely form where the lithosphere is  $\sim 10$  to 40 km thick, while many oval-shaped features called coronae, which are enigmatic volcanic-tectonic constructs, are likely to form where the lithosphere is  $\sim 10$  km or thinner. These features act as a load on the surface, causing the underlying plate to bend. We located the domes that show evidence of flexure and matched topographic data to an analytic model with a curve-fitting algorithm to determine the thickness of the idealized elastic plate. We then used a model of rock mechanics to infer the thickness of the real plate and thus the temperature gradient within the plate and the heat flow to the surface. Our results for elastic thickness at steep-sided domes matched prior predictions, supporting the hypothesis that plate bending influences the shapes and sizes of volcanic features on Venus.

## 1 Introduction

Properties of the lithosphere set the upper boundary condition for the evolution of planetary interiors. Interior dynamics in turn govern surface conditions over geologic time via volcanism, tectonics, and atmospheric outgassing (e.g., Foley & Driscoll, 2016; Smrekar et al., 2018). Venus's lithosphere is currently poorly understood, but we can use surface observations to learn about the interior and evolution of Earth's "evil twin". In particular, the elastic thickness of the lithosphere might control the morphology of volcanoes. McGovern et al. (2013) used two different magma ascent criteria to explore how coronae, steep-sided domes, and large conical edifices would form. Steep-sided domes, also called "pancake domes," appear nearly circular and flat from above (e.g., Gleason et al., 2010). This peculiar morphology is usually attributed to siliceous (dacitic and/or rhyolitic) volcanism (e.g., Head et al., 1991; Pavri et al., 1992). However, other studies suggest that the radar properties of these domes are more similar to basaltic or andesitic flows (e.g., Ford, 1994; Plaut et al., 2004; Stofan et al., 2000). In any case, steep-sided domes may most likely form at regions with elastic thicknesses of  $\sim 10\text{--}40$  km as shown in Figure 1 (McGovern et al., 2013). However, this hypothesis has not yet been confirmed via measurements of the actual elastic thickness.

Coronae are oval-shaped features with annular fractures and complex topography (e.g., Smrekar & Stofan, 1997; Stofan et al., 1992). According to McGovern et al. (2013), volcanic features resembling some coronae were most likely to form at regions with the lowest elastic

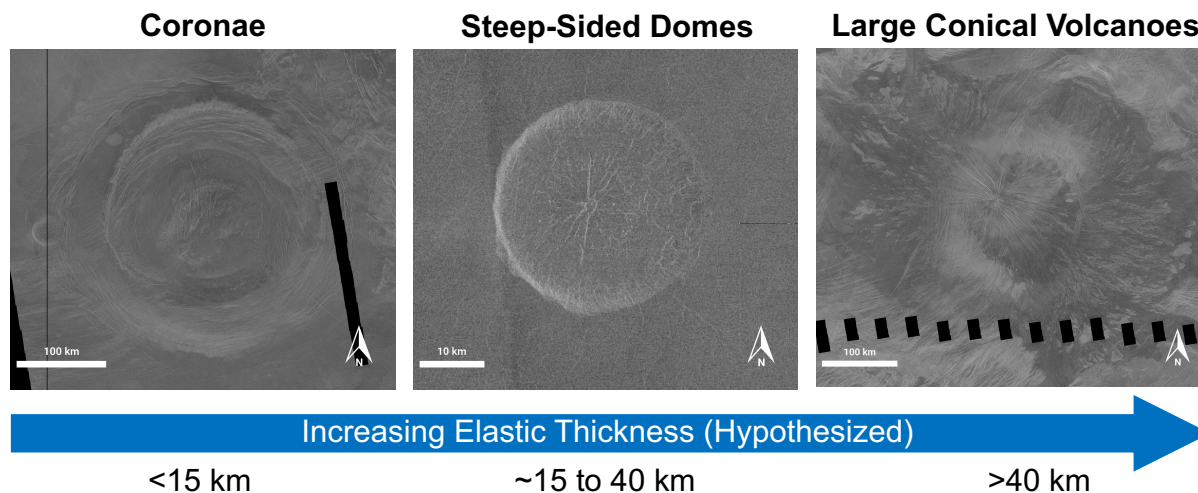


**Figure 1.** Steep-sided domes are predicted to form where the elastic thickness is thicker than at coronae but thinner than at large conical volcanoes (McGovern et al, 2013). These images were taken in JMARS using SAR imagery from NASA Magellan illuminated from the left. Black regions indicate missing data. The corona featured is Aramaiti Corona (82°E, 25.5°S), located next to Dome 2 in this paper. The dome featured is Dome 1 in this paper (151°E, 3°S). The large conical volcano featured is Tsiyostinako Mons (215°E, 15.5°S).

thicknesses:  $\sim 15$  km or less. Previous studies derived thin elastic thicknesses at coronae showing signs of lithospheric flexure. O'Rourke & Smrekar (2018) used newly available elevation models derived from stereo images (Herrick et al., 2012) to analyze topographic profiles of flexural signatures around coronae. That study used plate bending models of both broken and continuous (unbroken) elastic plates to estimate elastic thickness and heat flow. They determined the heat flow at all of these locations based on a conversion from elastic to mechanical thicknesses using an assumed rheology for the lithosphere. Overall, they found elastic thicknesses of  $\sim 5$  to 15 km at most coronae, corresponding to heat flows  $>95$  mW/m<sup>2</sup>. This result was somewhat unexpected because most models for the thermal evolution of Venus predict that the average surface heat flow is  $\sim 40$  mW/m<sup>2</sup> today with spikes to  $\sim 60$  mW/m<sup>2</sup> possible in the last billion years (e.g., Armann & Tackley, 2012; Gillmann & Tackley, 2014; Noack et al., 2012; O'Rourke & Korenaga, 2015; Weller & Kiefer, 2020). In contrast, the average surface heat flow for Earth is  $\sim 86$  mW/m<sup>2</sup> now (Jaupart et al., 2007).

Large conical volcanoes are predicted to form mostly at regions with elastic thicknesses of 40 km or greater. We did not explore large conical volcanoes in this study because the topographic signatures of flexure necessary for our analysis are not visible at those locations. McGovern & Solomon (1997) explained that flexural moats around these large volcanoes were likely filled in by lava flows from the large volcanoes themselves. Even using the stereo-derived topography, we were unable to find flexural signatures that would permit the analyses used for coronae previously and for steep-sided domes in this study.

Russell & Johnson (2019) previously studied lithospheric flexure at one steep-sided dome. Specifically, they obtained topographic profiles radiating from a flexural moat around Narina Tholi. Their pioneering analyses revealed a very thin lithosphere at this location, with an elastic thickness of  $\sim 2$ – $3$  km. This result was somewhat expected given that Narina Tholi is

located directly on the rim of Aramaiti Corona, which have been found to be associated with <15 km-thick lithosphere (O'Rourke & Smrekar 2018; Johnson & Sandwell 1994). They concluded that Narina Tholi was emplaced during the late stages of the formation of Aramaiti Corona when the heat flow from the interior to the surface was particularly elevated. Recently, Gülcher et al. (2020) argued that plume-lithosphere interaction at Aramaiti Corona could be actively occurring today. Generally speaking, the geologic context of individual volcanic features is critical to interpreting measurements of elastic thickness from lithospheric flexure. In this study, we conducted a global survey of lithospheric flexure at steep-sided domes to assemble a database of elastic thicknesses and other properties for this class of features.

## 2 Materials and Methods

### 2.1 Topographic Profiles

We accessed a database of volcanic features on Venus (Pavri et al., 1992) to find the latitude and longitude of steep-sided domes. We used JMARS to locate these domes using Magellan Synthetic Aperture Radar (SAR) data. Only the domes we were able to definitively identify in both the SAR imagery and topography (75 out of ~150 candidates) were used in this study. The remaining candidates were disregarded if we were unable to locate them in the imagery, if there was a gap in the topography data, or if the topography data was not of a high enough quality to distinguish the dome. We drew 8 topographic profiles at increments of  $\sim 45^\circ$  around 75 steep-sided domes. The profile extending north ( $0^\circ$ ) is labelled profile 1, and the labelling numbers increase clockwise through profile 8 (Figure 2a). Wherever possible, the topographic profiles were taken using stereo-derived topography, which covers about 20% of the surface at horizontal and vertical resolutions of  $\sim 1$  km and  $\sim 100$  m, respectively (Herrick et al., 2012). Topography from areas without stereo coverage was extracted from the global topographic data record (GTDR) collected from the Magellan mission. The horizontal resolution is more than an order-of-magnitude worse than the stereo dataset at  $\sim 10$ – $20$  km (Ford & Pettengill, 1992). The profiles were drawn starting at approximately the edge of the dome and extended out  $\sim 800$  km. We imported the topographic profiles into MATLAB and trimmed them to begin at the lowest point in the moat around the dome. The elevation values were normalized to 0 m at the start by subtracting the first elevation value.

Only the profiles that showed clear evidence of flexural signatures were chosen for further analysis. These signatures appear as a moat surrounding the dome, followed by a rise in elevation leading to a forebulge, before the topography eventually flattens out (Figure 2b). Some profiles encountered interfering topography such as craters or other mountains and were either discarded or truncated. We found flexural signatures in 29 profiles from 14 different domes. These domes were chosen for further analysis (Figure 2c). We noted the type of terrain in which each dome was located: tesserae or plains. Additionally, we determined which domes were in close proximity to other features such as coronae. Fotla Corona lies south of dome 75, interacting with only profiles 3, 4, 5, and 6. We thus divide dome 75 into 75a (profiles 1, 2, and 8) and 75b (profiles 3–6) to indicate which profiles intersect the corona and which do not.

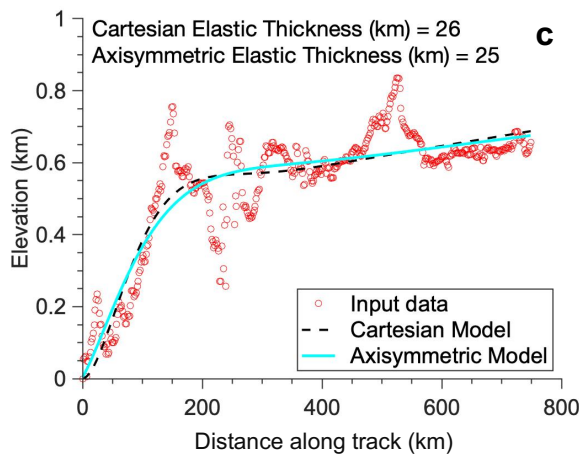
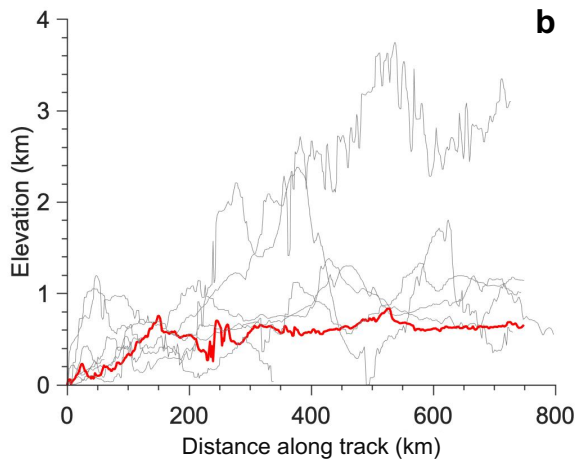
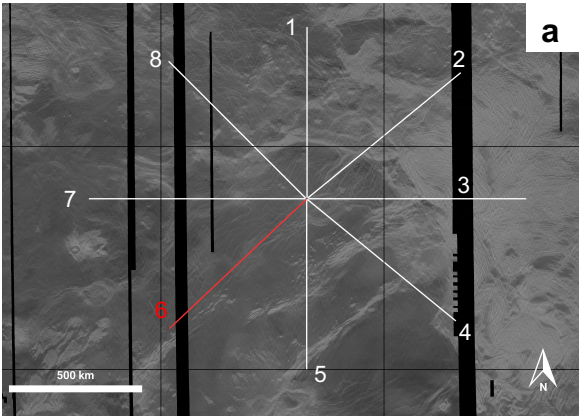


**Figure 2.** Profiles that show signs of flexure are chosen for further analysis with the curve-fitting algorithm. (a) Profiles drawn around dome 16 (66 °E, 37.5 °N) in JMARS. The profile that shows signs of flexure (profile 6) is highlighted in red, which is the only profile that does not cover heavily fractured or tectonized terrain. (b) All topographic profiles, including those that are not amenable to a flexural interpretation (grey). The profile that was later analyzed is again in red. The profiles begin at the lowest elevation point in the flexural moat surrounding the dome. (c) Cartesian and axisymmetric curve fits to the shape of profile 6 around dome 16.

## 2.2 Flexure and Elastic Thickness

We used standard models of lithospheric flexure to infer the elastic thickness from topography. Steep-sided domes are  $\sim 1$  km tall (e.g., Gleason et al., 2010; Pavri et al., 1992) and thus produce vertical loads of order  $\sim 1$  MPa, which are not sufficient to break the lithosphere by themselves. In general, we assume that the lithosphere is continuous (unbroken) and that in-plane (horizontal) forces are negligible. A differential equation describes the resulting deformation under a vertical load (Turcotte & Schubert, 2002):

$$D\nabla^2\nabla^2w + \Delta\rho gw = q(r), \quad (1)$$

where  $D$  is the flexural rigidity,  $w$  is the displacement from the pre-flexure elevation,  $q$  is the vertical load per unit area, and  $r$  is the radial distance along track. Table S1 defines the constants used in our analysis such as the density contrast across the lithosphere between the atmosphere and upper mantle ( $\Delta\rho$ ) and gravitational acceleration ( $g$ ). We can solve the governing equation in both Cartesian and axisymmetric (cylindrical) geometry. The axisymmetric version is preferred because the steep-sided domes are relatively small with diameters comparable to the elastic thickness. In other words, the horizontal curvature of the load is important to assessing the flexural response of the plate. In contrast, switching the assumed geometry for flexural analyses of much larger features such as coronae changes the derived elastic thicknesses by  $\sim 20\%$  or less (e.g., Johnson & Sandwell, 1994; O'Rourke & Smrekar, 2018).

We fit analytic solutions to Equation 1 to the topographic profiles. In axisymmetric geometry,  $q(r) = q_0$  is a constant for  $r$  less than the diameter of the dome ( $R$ ) and zero elsewhere. The solution for  $r \geq R$ , outside of the dome, is (Johnson & Sandwell, 1994):

$$w(r) = -\frac{q_0}{\Delta\rho g} \left(\frac{R}{\alpha}\right) \left[ \text{ber}'\left(\frac{R}{\alpha}\right) \text{ker}\left(\frac{r}{\alpha}\right) - \text{bei}'\left(\frac{R}{\alpha}\right) \text{kei}\left(\frac{r}{\alpha}\right) \right] + sr. \quad (2)$$

Here  $\alpha$  is the flexural parameter and  $s$  accounts for any regional slope. This equation uses the Kelvin functions  $\text{ber}$ ,  $\text{ker}$ ,  $\text{bei}$ , and  $\text{kei}$  with apostrophes indicating first-derivatives. The Cartesian model treats the dome as an end load so  $q(r) = 0$  Pa everywhere along the profile. The standard Cartesian solution is (Turcotte & Schubert, 2002):

$$w(r) = w_0 \left\{ 1 - e^{-\frac{r}{\alpha}} \left[ \cos\left(\frac{r}{\alpha}\right) + \sin\left(\frac{r}{\alpha}\right) \right] \right\} + sr, \quad (3)$$

where  $w_0$  is the maximum displacement (i.e., at the start of the profile in the flexural trough). We used the `fminsearch` curve-fitting algorithm in MATLAB (Lagarias et al., 1998) to find the best-fit parameters for each model. We seed the curve-fitting algorithm with initial guesses: the distance along track to the forebulge for  $\alpha$ ; the maximum normalized elevation divided by the total length of the profile for  $s$ ; the difference between the maximum and minimum elevations for  $w_0$  in the Cartesian model, and 1 MPa for  $q_0$  in the axisymmetric model.

The elastic thickness is extracted from the best-fit flexural parameters derived in both geometries. Specifically, the elastic thickness ( $h_e$ ) is (Turcotte & Schubert 2002):

$$h_e = \left[ \frac{3}{E} (\Delta\rho g \alpha^4) (1 - \nu^2) \right]^{\frac{1}{3}}, \quad (4)$$

where  $E$  is Young's modulus (100 GPa) and  $\nu$  is Poisson's ratio (0.25). This equation is derived from the standard definitions of the flexural rigidity,  $D = (Eh_e^3)/[12(1 - \nu^2)]$ , and the flexural parameter,  $\alpha = [4D/(\Delta\rho g)]^{1/4}$ . The curve-fitting algorithm returns formal uncertainties for all parameters. We use a Monte Carlo method to propagate the uncertainties on  $\alpha$  to estimate the "1-sigma" uncertainties on the best-fit elastic thickness. O'Rourke & Smrekar (2018) used a sophisticated Markov chain Monte Carlo to fit flexural models to topography, but also demonstrated that simpler curve-fitting algorithms yield equivalent results.

### 2.3 Mechanical Thickness and Heat Flow

We used a yield stress envelope to calculate the mechanical thickness, surface heat flow, and thermal gradient at each dome. In an idealized elastic plate, the horizontal stress varies linearly between the maximum extensional stress at the top of the plate to the maximum compressional stress at its lower boundary. The real, mechanical plate is thicker than the elastic lithosphere because brittle and ductile failure occur at the top and bottom of the plate, respectively. The total bending moments for the idealized elastic and mechanical plates should be equal, allowing us to convert elastic thickness estimates to mechanical thickness estimates (e.g., Brown & Grimm, 1996; McNutt, 1984). We used the maximum curvature ( $d^2w/dr^2$ ) of the elastic plate in these calculations. We determined that the axisymmetric geometry was the most accurate and chose to move forward analyzing the mechanical thicknesses for only this model.

Because we know that the mechanical plate begins at the surface and ends where the temperature is high enough to cause ductile flow, we can use the mechanical thickness to determine the thermal gradient. The equation used to obtain the thermal gradient is:

$$\frac{dT}{dz} = \frac{T_C - T_S}{h_m}, \quad (5)$$

$T_S = 740$  K is the surface temperature, and  $h_m$  is the mechanical thickness.  $T_C$  is the critical temperature above which ductile flow begins, which depends on the rheology of the material. Table 1 reports the results calculated using a dry olivine rheology ( $T_C \sim 1013$  K). Table S2 lists values calculated using two rheological models for dry diabase (Mackwell et al., 1998). We then calculate the surface heat flow:

$$F_s = k_c \frac{dT}{dz}, \quad (6)$$

with  $k_c = 4$  W/m/K being the thermal conductivity of the crust (Turcotte & Schubert, 2002).

### 2.4 Agreement with Gravity Data

We determined the level of agreement between our derived elastic thicknesses and those in the global map derived from admittance, which is the ratio of gravity to topography (Figure 14 in Anderson & Smrekar, 2006). By searching within an oval the size of the resolution of the gravity, we counted the number of pixels for which the values match those from our study. Domes where >50%, 0–50%, and 0% of the pixels agree within  $\pm 20$  km are considered to have “excellent”, “good”, and “no” agreement, respectively. Two domes (21 and 51) are partially within areas where elastic thickness could not be retrieved from admittance data, which might artificially lower the level of agreement.

**Table 1**

List of all domes with at least one topographic profile amenable to a flexural interpretation. From left to right, the first four columns show the index number, diameter, longitude, and latitude of each dome. Elastic thicknesses ( $h_e$ ) were calculated using plate-bending models with axisymmetric and Cartesian geometry. Mechanical thicknesses ( $h_m$ ) and surface heat flows ( $F_s$ ) were derived using a yield stress envelope for dry olivine. Our estimates of elastic thickness were compared with the map in Anderson & Smrekar (2006) using the scale explained in the main text. Quoted uncertainties represent one standard deviation. Results from multiple profiles were averaged using Monte Carlo error propagation.

<b>Dome</b>	<b>Dia. (km)</b>	<b>Lon. (°)</b>	<b>Lat. (°)</b>	<b>Axi. <math>h_e</math> (km)</b>	<b>Cart. <math>h_e</math> (km)</b>	<b><math>h_m</math> (km)</b>	<b><math>F_s</math> (mW/m<sup>2</sup>)</b>	<b>Agreement with Global Map</b>	<b>Geologic Context</b>
1	35	151	-3	37.6 ± 1.5	40.9 ± 1.3	38.1 ± 1.5	28.7 ± 1.1	Good	Plains
2	40	80	-26	4.4 ± 0.2	3.2 ± 0.1	5.3 ± 0.1	279.4 ± 13.7	Excellent	Near Aramaiti Corona
5	25	63	28	16.8 ± 1.1	20.0 ± 1.0	17.3 ± 1.1	64.0 ± 3.6	Excellent	Plains
7	30	79	43	16.9 ± 0.6	17.0 ± 0.6	20.3 ± 0.5	61.3 ± 1.6	Excellent	Tessera
13	25	69	28	15.2 ± 2.3	18.5 ± 2.5	16.3 ± 2.0	68.1 ± 8.5	Excellent	Tessera
16	30	66	38	23.7 ± 1.4	26.5 ± 1.3	24.4 ± 1.3	44.9 ± 2.4	Excellent	Plains
20	20	85	57	28.6 ± 1.5	40.3 ± 1.8	29.7 ± 1.4	36.8 ± 1.7	Excellent	Plains
21	25	98	50	32.9 ± 3.6	33.0 ± 2.4	33.5 ± 3.5	33.0 ± 3.5	Good	Plains
22	25	342	48	41.2 ± 2.9	52.7 ± 2.9	41.7 ± 2.8	26.3 ± 1.8	None	Plains
26	50	312	34	8.5 ± 0.7	7.5 ± 0.8	10.0 ± 0.5	109.3 ± 5.9	None	Plains
32	20	314	25	16.9 ± 1.0	14.9 ± 0.9	17.6 ± 0.9	62.3 ± 3.3	Good	Plains
51	20	247	-13	2.9 ± 0.1	2.2 ± 0.1	5.1 ± 0.1	216.3 ± 5.1	Good	Near corona
64	30	264	-35	3.4 ± 0.3	4.3 ± 0.3	5.8 ± 0.3	190.1 ± 9.2	Excellent	Near corona
75 a	25	162	-58	19.5 ± 0.1	22.0 ± 0.7	20.7 ± 0.6	91.2 ± 4.8	Good	Plains
75 b	25	162	-58	14.0 ± 0.3	16.0 ± 0.4	15.0 ± 0.4	103.9 ± 3.6	Good	Near Fotla Corona

### 3 Results

Table 1 collects the results for all profiles in this study. Out of the 14 domes that showed evidence of flexure, 6 were located within the swaths of stereo data. In order to not overrepresent domes for which multiple profiles showed flexural signatures, we calculated the average values and uncertainties for all profiles around each dome using a Monte Carlo technique. The values in Table 1 for domes 2, 5, 7, 75a, and 75b are the averages of multiple profiles around those domes that were amenable to flexural interpretations. Table S3 lists the parameters derived from each individual profile. When considering all profiles, we found an average elastic thickness of  $\sim 16$  and 15 km for a continuous plate using the Cartesian and axisymmetric models, respectively.

There was a significant difference in derived elastic thicknesses based on whether or not the domes were located in close proximity to coronae, which have been found mostly in regions with thin elastic thicknesses (Figure 3a). Profiles around domes 2, 7, 51, 64, and 75b were near coronae (within  $\sim 800$  km, the length of the topographic profiles). Most of these profiles did have elastic thicknesses below the average expected for steep-sided domes. The average elastic thickness for profiles that are near coronae ranged from  $\sim 2$ –16 km using Cartesian geometry, and  $\sim 3$ –14 km using axisymmetric geometry. Profiles around domes 1, 5, 13, 16, 20, 21, 22, 26, 32, and 75a were not located near coronae. These profiles yielded average elastic plate thicknesses ranging from  $\sim 8$ –41 km using the Cartesian model and  $\sim 9$ –38 km using the axisymmetric model. Our derived mechanical thicknesses were  $\sim 20\%$  larger than the elastic thicknesses, while mechanical thicknesses can be a factor of  $\sim 2$  larger than elastic thicknesses derived at coronae (O'Rourke & Smrekar 2018). This difference is due to the fact that domes are associated with smaller loads and thicker lithosphere than coronae, thus leading to a smaller plate curvature.

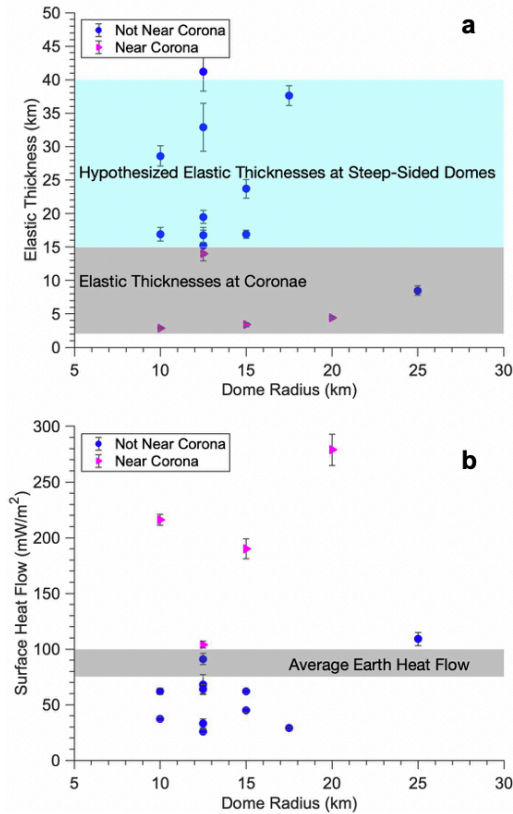


**Figure 3:** Derived properties at all domes analyzed in our study. Error bars indicate the average standard deviation (“1-sigma”) calculated from all profiles around the dome. Domes near coronae are represented as pink triangles, while blue circles show domes that are not near coronae. (a) Elastic thicknesses at each dome calculated using the axisymmetric model. Color shading indicates the predicted ranges for domes (blue) and coronae (grey) from Figure 1. (b) Surface heat flows calculated using elastic thicknesses and curvatures from the axisymmetric model and a yield stress envelope for dry olivine.

We reproduced the results around Narina Tholi from Russell & Johnson (2019). This dome is directly on the margin of Aramaiti Corona and thus has a low elastic thickness. In our analysis, Narina Tholi is referred to as dome 2. We trimmed our profiles to extend  $\sim 100$  km from the flexural moat to match that of Russell & Johnson (2019). These topographic profiles also show signs of lithospheric flexure. The elastic thickness at the location of dome 2 is low:  $\sim 3$  km using Cartesian geometry and  $\sim 4$  km using axisymmetric geometry. This low estimate of elastic thickness for the dome agrees with the values of  $\sim 2$ – $3$  km from Russell & Johnson (2019).

We also found a significant variance in surface heat flow dependent on whether the profiles were near coronae (Figure 3b). Those profiles that were close to coronae yielded surface heat flows ranging from  $\sim 104$ – $279$  mW/m<sup>2</sup>, ( $\sim 197$  mW/m<sup>2</sup> on average). Analyses of flexural signatures from topographic profiles that did not encounter coronae yielded heat flows of  $\sim 29$ – $109$  mW/m<sup>2</sup>. The average heat flow of  $\sim 57$  mW/m<sup>2</sup> for these domes is close to that predicted for Venus globally in some thermal evolution models (e.g., Gillmann & Tackley, 2014).

We determined the level of agreement between our derived values and those derived from gravity data. Out of 14 domes, 12 showed at least some agreement between our elastic thickness values and the gravity-derived values. Of these, 7 showed excellent agreement ( $>50\%$ ), another 5 domes showed good agreement ( $0$ – $50\%$ ), and 2 showed no agreement. There was no bias in the levels of agreement between domes that are near coronae or not.

#### 4 Discussion & Conclusions

We verified the hypothesis that steep-sided domes typically form at regions of elastic thickness between  $\sim 10$  and  $40$  km. The distribution of steep-sided domes can thus tell us about

the elastic thickness of the lithosphere on Venus (McGovern et al., 2013). Flexural signatures are not always visible as moats may have been filled in by later lava flows or other interfering events. Additionally, it might not be possible to collect reliable topographic profiles around domes that are close to other interfering topography such as craters or mountains. However, one may use the presence of steep-sided domes to infer that the elastic thickness should be between ~10 and 40 km at a given location. Lithospheric thickness can then act as a probe into the interior of the planet. Thus, the distribution of steep-sided domes on Venus is also a tool that future studies could use to constrain the regional and global heat flow out of the deep interior.

Domes located near coronae were associated with thin elastic lithosphere. Our results thus provide further evidence for thin elastic thickness at coronae. Our findings for elastic thickness were consistent with the regional elastic thicknesses derived from gravity data (Anderson & Smrekar, 2006) regardless of the proximity of domes to coronae. Profiles that are located near coronae had significantly lower mechanical thickness and thus higher average surface heat flows than those that were not near coronae.

While volcanic features are likely to form where the elastic thickness is within the hypothesized range, they appear to can form on thinner lithosphere as well. We did not consider factors such as tectonic history, geologic history, and rheology that could affect volcano morphology (e.g. Watts & Zhong, 2000). Where domes occur near coronae, it is generally impossible to determine relative ages, making the role of any localized heating associated with corona formation difficult to assess.

Further spacecraft exploration of Venus is urgently needed to improve our understanding of the Venusian interior. Stereo-derived topography proved to be an important dataset in the search for flexural signatures. Stereo data is only available for about 20% of Venus' surface, yet >40% of the flexural signatures around steep-sided domes were found using stereo data. The disproportionate number of signatures identified using stereo-derived topography suggests that flexural signatures do exist around other steep-sided domes but could not be seen in the lower-resolution Global Topographic Data Record. This study also supported the idea that flexural signatures around steep-sided domes provide reliable estimates of lithospheric thickness. Improved data from new missions would reveal different features and allow us to conduct more precise studies. Future missions to Venus to gather high-resolution radar images, topography, and gravity data on a global scale are necessary to understand the interior and evolution of Earth's nearest neighbor.

## **Acknowledgments and Data**

This work was supported by NASA Solar System Workings (grant # 811073.02.35.04.55). Data supporting the conclusions are located in the tables and supporting information. Imagery and topography from the NASA Magellan mission, including stereo-derived topography, are available in JMARS (<https://jmars.asu.edu/>). Data sharing is not applicable to this article as no new data were created or analyzed in this study. Imagery and topography data from the NASA Magellan Mission used to create the figures and tables are available from the NASA Planetary Data System (<https://pds-geosciences.wustl.edu/missions/magellan/index.htm>).

## References

- Anderson, F. S., & Smrekar, S. E. (2006). Global mapping of crustal and lithospheric thickness on Venus. *Journal of Geophysical Research*, *111*(E8), E08006. <https://doi.org/10.1029/2004JE002395>
- Armann, M., & Tackley, P. J. (2012). Simulating the thermochemical magmatic and tectonic evolution of Venus's mantle and lithosphere: Two-dimensional models. *Journal of Geophysical Research*, *117*(E12), E12003. <https://doi.org/10.1029/2012JE004231>
- Brown, C. D., & Grimm, R. E. (1996). Lithospheric rheology and flexure at Artemis Chasma, Venus. *Journal of Geophysical Research: Planets*, *101*(E5), 12697–12708. <https://doi.org/10.1029/96JE00834>
- Foley, B. J., & Driscoll, P. E. (2016). Whole planet coupling between climate, mantle, and core: Implications for rocky planet evolution. *Geochemistry, Geophysics, Geosystems*, *17*(5), 1885–1914. <https://doi.org/10.1002/2015GC006210>
- Ford, P. G. (1994). Radar Scattering Properties of Steep-Sided Domes on Venus. *Icarus*, *112*(1), 204–218. <https://doi.org/10.1006/icar.1994.1178>
- Ford, P. G., & Pettengill, G. H. (1992). Venus topography and kilometer-scale slopes. *Journal of Geophysical Research*, *97*(E8), 13103. <https://doi.org/10.1029/92JE01085>
- Gillmann, C., & Tackley, P. (2014). Atmosphere/mantle coupling and feedbacks on Venus. *Journal of Geophysical Research: Planets*, *119*(6), 1189–1217. <https://doi.org/10.1002/2013JE004505>
- Gleason, A. L., Herrick, R. R., & Byrnes, J. M. (2010). Analysis of venusian steep-sided domes utilizing stereo-derived topography. *Journal of Geophysical Research E: Planets*, *115*(6), 1–9. <https://doi.org/10.1029/2009JE003431>
- Gülcher, A. J. P., Gerya, T. V., Montési, L. G. J., & Munch, J. (2020). Corona structures driven by plume–lithosphere interactions and evidence for ongoing plume activity on Venus. *Nature Geoscience*, *13*(August). <https://doi.org/10.1038/s41561-020-0606-1>
- Head, J. W., Campbell, D. B., Elachi, C., Guest, J. E., Mckenzie, D. P., Saunders, R. S., et al. (1991). Venus volcanism: Initial analysis from Magellan data. *Science*, *252*(5003), 276–288. <https://doi.org/10.1126/science.252.5003.276>
- Herrick, R. R., Stahlke, D. L., & Sharpton, V. L. (2012). Fine-scale Venusian topography from Magellan stereo data. *Eos*, *93*(12), 125–126. <https://doi.org/10.1029/2012EO120002>
- Jaupart, C., Labrosse, S., & Mareschal, J.-C. (2007). Temperatures, Heat and Energy in the Mantle of the Earth. In *Treatise on Geophysics* (pp. 253–303). Elsevier. <https://doi.org/10.1016/B978-044452748-6.00114-0>
- Johnson, C. L., & Sandwell, D. T. (1994). Lithospheric flexure on Venus. *Geophysical Journal International*, *119*(2), 627–647. <https://doi.org/10.1111/j.1365-246X.1994.tb00146.x>
- Lagarias, J. C., Reeds, J. A., Wright, M. H., Wright P. E. (1998). Convergence properties of the Nelder-Mead simplex method in low dimensions. *SIAM Journal on Optimization*, *9*, 112–147. doi:10.1137/s1052623496303470

- Mackwell, S. J., Zimmerman, M. E., & Kohlstedt, D. L. (1998). High-temperature deformation of dry diabase with application to tectonics on Venus. *Journal of Geophysical Research: Solid Earth*, 103(B1), 975–984. <https://doi.org/10.1029/97JB02671>
- McGovern, P. J., & Solomon, S. C. (1997). Filling of flexural moats around large volcanoes on Venus: Implications for volcano structure and global magmatic flux. *Journal of Geophysical Research E: Planets*, 102(E7), 16303–16318. <https://doi.org/10.1029/97JE01318>
- McGovern, P. J., Rumpf, M. E., & Zimbelman, J. R. (2013). The influence of lithospheric flexure on magma ascent at large volcanoes on Venus. *Journal of Geophysical Research: Planets*, 118, 2423–2437. <https://doi.org/10.1002/2013JE004455>
- McNutt, M. K. (1984). Lithospheric flexure and thermal anomalies. *Journal of Geophysical Research: Solid Earth*, 89(B13), 11180–11194. <https://doi.org/10.1029/JB089iB13p11180>
- Noack, L., Breuer, D., & Spohn, T. (2012). Coupling the atmosphere with interior dynamics: Implications for the resurfacing of Venus. *Icarus*, 217(2), 484–498. <https://doi.org/10.1016/j.icarus.2011.08.026>
- O’Rourke, J. G., & Korenaga, J. (2015). Thermal evolution of Venus with argon degassing. *Icarus*, 260, 128–140. <https://doi.org/10.1016/j.icarus.2015.07.009>
- O’Rourke, J. G., & Smrekar, S. E. (2018). Signatures of Lithospheric Flexure and Elevated Heat Flow in Stereo Topography at Coronae on Venus. *Journal of Geophysical Research: Planets*, 123(2), 369–389. <https://doi.org/10.1002/2017JE005358>
- Pavri, B., Head, J. W., Klose, K. B., & Wilson, L. (1992). Steep-sided domes on Venus: Characteristics, geologic setting, and eruption conditions from Magellan data. *Journal of Geophysical Research*, 97(E8), 13445. <https://doi.org/10.1029/92JE01162>
- Plaut, J. J., Anderson, S. W., Crown, D. A., Stofan, E. R., & van Zyl, J. J. (2004). The unique radar properties of silicic lava domes. *Journal of Geophysical Research E: Planets*, 109(3), 1–12. <https://doi.org/10.1029/2002je002017>
- Russell, M. B., & Johnson, C. L. (2019). Lithospheric Flexure Modeling at Narina Tholi: Evidence for a Locally Thinned Lithosphere. In *Lunar and Planetary Science Conference* (p. 2896). Retrieved from <https://www.hou.usra.edu/meetings/lpsc2019/pdf/2896.pdf>
- Smrekar, S. E., & Stofan, E. R. (1997). Corona Formation and Heat Loss on Venus by Coupled Upwelling and Delamination. *Science*, 277(5330), 1289–1294. <https://doi.org/10.1126/science.277.5330.1289>
- Smrekar, S. E., Davaille, A., & Sotin, C. (2018). Venus Interior Structure and Dynamics. *Space Science Reviews*, 214(5), 88. <https://doi.org/10.1007/s11214-018-0518-1>
- Stofan, E. R., Sharpton, V. L., Schubert, G., Baer, G., Bindschadler, D. L., Janes, D. M., & Squyres, S. W. (1992). Global distribution and characteristics of coronae and related features on Venus: Implications for origin and relation to mantle processes. *Journal of Geophysical Research*, 97(E8), 13347. <https://doi.org/10.1029/92JE01314>
- Stofan, E. R., Anderson, S. W., Crown, D. A., & Plaut, J. J. (2000). Emplacement and composition of steep-sided domes on Venus. *Journal of Geophysical Research E: Planets*, 105(E11), 26757–26771. <https://doi.org/10.1029/1999JE001206>

Turcotte, D. L., & Schubert, G. (2002). *Geodynamics*. New York: Cambridge University Press.

Watts, A. B., & Zhong, S. (2000). Observations of flexure and the rheology of oceanic lithosphere. *Geophysical Journal International*, 142(3), 855-875. doi:10.1046/j.1365-246x.2000.00189.x

Weller, M. B., & Kiefer, W. S. (2020). The Physics of Changing Tectonic Regimes: Implications for the Temporal Evolution of Mantle Convection and the Thermal History of Venus. *Journal of Geophysical Research: Planets*, 125(1), 2019JE005960. <https://doi.org/10.1029/2019JE005960>

**A Global Survey of Lithospheric Flexure at Steep-Sided Domical Volcanoes on Venus Reveals Intermediate Elastic Thicknesses**

M. E. Borrelli<sup>1</sup>, J. G. O'Rourke<sup>1</sup>, S. E. Smrekar<sup>2</sup>, C. M. Ostberg<sup>3</sup>

<sup>1</sup>Arizona State University, School of Earth and Space Exploration, Tempe, AZ.

<sup>2</sup>Jet Propulsion Laboratory, California Institute of Technology, Pasadena, CA.

<sup>3</sup>University of California, Department of Earth and Planetary Sciences, Riverside, CA.

**Contents of this file**

Tables S1 to S3, Figure S1

**Additional Supporting Information (Files uploaded separately)**

Captions for Datasets S1 to S2

**Introduction**

This Supporting Information includes tables that complement the main text, along with datasets that could be used to reproduce our results. All topographic profiles were extracted from the Magellan global topographic data record (GTDR) and, where available, stereo-derived digital elevation maps using JMARS.

**Table S1**

Values of constants used in curve-fitting functions and calculations, which were taken from Johnson & Sandwell (1994) except the rheological laws for dry olivine and diabase are from McNutt (1984) and Mackwell et al. (1998), respectively.

Constant	Definition	Value	Units
$g$	Gravitational acceleration at the surface of Venus	8.87	m/s <sup>2</sup>
$E$	Young's modulus	100	GPa
$\Delta\rho$	Density contrast across the lithosphere	3300	kg/m <sup>3</sup>
$\nu$	Poisson's ratio	0.25	
$k_c$	Thermal conductivity of the lithosphere	4	W/m/K
$T_c$	Critical temperature for dry olivine (above which <a href="#">the</a> ductile strength is $\leq 50$ MPa)	1013	K
$T_c$	Critical temperature for dry diabase (Columbia)	1013	K
$T_c$	Critical temperature for dry diabase (Maryland)	961	K
$T_s$	Surface temperature on Venus	740	K

**Table S2**

List of all domes with at least one topographic profile amenable to a flexural interpretation. From left to right, the first four columns show the index number, diameter, longitude, and latitude of each dome. Mechanical thicknesses ( $h_e$ ) and surface heat flows ( $F_s$ ) were derived using yield stress envelopes for two types of dry diabase (Mackwell et al., 1998).

Dome	Dia. (km)	Lon (°)	Lat (°)	Maryland		Columbia	
				$h_m$ (km)	$F_s$ (mW/m <sup>2</sup> )	$h_m$ (km)	$F_s$ (mW/m <sup>2</sup> )
1	35	151.0	-3.0	38.1 ± 1.5	28.7 ± 1.1	38.1 ± 1.5	28.7 ± 1.1
2	40	80.0	-26.0	5.3 ± 0.1	279.7 ± 13.9	5.3 ± 0.1	279.0 ± 13.5
5	30	63.0	28.0	17.3 ± 1.1	63.9 ± 3.7	17.3 ± 1.1	63.9 ± 3.6
7	30	79.0	42.5	20.3 ± 0.5	61.3 ± 1.6	20.3 ± 0.5	61.3 ± 1.6
13	25	68.5	28.0	16.3 ± 0.5	68.1 ± 8.4	16.2 ± 2.0	68.3 ± 8.5
16	30	66.0	37.5	24.3 ± 1.3	45.0 ± 2.4	24.4 ± 1.3	44.9 ± 2.4
20	20	85.0	57.0	29.7 ± 1.4	36.8 ± 2.7	29.7 ± 1.4	36.8 ± 1.7
21	25	97.5	50.0	33.6 ± 3.4	32.9 ± 3.4	33.5 ± 3.4	32.9 ± 3.4
22	25	342.0	48.0	41.7 ± 2.8	26.3 ± 1.8	41.8 ± 2.8	26.3 ± 1.8
26	50	311.5	34.0	10.0 ± 0.5	109.3 ± 5.9	10.0 ± 0.6	109.2 ± 6.2
32	20	314.0	25.0	17.6 ± 0.9	62.3 ± 3.3	17.6 ± 0.9	62.4 ± 3.3
51	20	247.0	-12.5	5.1 ± 0.1	216.3 ± 5.2	5.1 ± 0.1	216.3 ± 5.2
64	30	264.0	-35.0	5.8 ± 0.3	190.0 ± 9.1	5.8 ± 0.3	190.1 ± 9.1
75 a	25	162.0	-58.0	20.7 ± 0.6	91.1 ± 4.8	20.1 ± 0.6	91.1 ± 4.7
75 b	25	162.0	-58.0	15.0 ± 0.4	104.0 ± 3.6	15.0 ± 0.4	104.0 ± 3.6

**Table S3**

*Results from each individual profile for steep-sided domes with multiple profiles that were amenable to flexural interpretation.*

Dome	Profile	Axi. $h_e$ (km)	Cart. $h_e$ (km)	Dry Olivine		Maryland Diabase		Columbia Diabase	
				$h_m$ (km)	$F_s$ (mW/m <sup>2</sup> )	$h_m$ (km)	$F_s$ (mW/m <sup>2</sup> )	$h_m$ (km)	$F_s$ (mW/m <sup>2</sup> )
2	1	5.2 ± 0.1	4.6 ± 0.2	6.3 ± 0.1	173.6 ± 3.0	3.0 ± 6.3	173.6 ± 3.0	6.4 ± 0.1	173.6 ± 3.0
2	2	4.7 ± 1.0	3.0 ± 0.2	5.3 ± 0.9	210.9 ± 38.5	40.5 ± 5.3	211.4 ± 40.2	5.3 ± 0.9	211.9 ± 40.5
2	3	9.9 ± 0.5	7.6 ± 0.6	11.5 ± 0.4	94.8 ± 3.3	3.4 ± 11.5	94.8 ± 3.4	11.5 ± 0.4	94.9 ± 3.4
2	4	2.5 ± 0.2	2.1 ± 0.1	3.2 ± 0.2	339.4 ± 17.2	17.5 ± 3.2	338.9 ± 17.3	3.2 ± 0.2	339.1 ± 17.5
2	5	1.3 ± 0.3	1.2 ± 0.2	2.1 ± 0.3	547.6 ± 99.4	100.8 ± 2.1	545.3 ± 97.1	2 ± 0.3	549.4 ± 100.8
2	6	2.3 ± 0.1	1.5 ± 0.1	3.3 ± 0.1	334.5 ± 10.4	10.6 ± 3.3	334.1 ± 10.4	3.3 ± 0.1	334.7 ± 10.6
2	7	2.2 ± 0.1	1.9 ± 0.1	2.8 ± 0.1	394.6 ± 8.9	9.0 ± 2.8	394.4 ± 9.0	2.8 ± 0.1	394.7 ± 9.0
2	8	7.4 ± 0.4	4.5 ± 0.3	7.9 ± 0.4	139.5 ± 6.3	6.3 ± 7.8	139.5 ± 6.3	7.9 ± 0.4	139.4 ± 6.3
5	1	18.3 ± 1.8	23.3 ± 1.9	18.7 ± 1.8	59.0 ± 5.7	5.6 ± 18.7	59.0 ± 5.7	18.7 ± 1.8	58.8 ± 5.6
5	2	15.2 ± 1.1	16.4 ± 0.8	15.9 ± 1.1	69.1 ± 4.6	4.7 ± 15.9	69.0 ± 4.6	15.9 ± 1.1	69.1 ± 4.7
7	4	24.9 ± 1.0	26.8 ± 1.0	27.3 ± 0.8	40.1 ± 1.2	1.2 ± 27.2	40.1 ± 1.3	27.3 ± 0.8	40.1 ± 2.1
7	5	8.9 ± 0.6	7.7 ± 0.6	13.3 ± 0.5	82.5 ± 3.0	3.0 ± 13.3	82.5 ± 3.0	13.2 ± 0.5	82.6 ± 3.0
75	1	26.5 ± 0.9	30.3 ± 1.0	27.6 ± 0.9	39.6 ± 1.2	1.2 ± 27.6	39.6 ± 1.2	27.6 ± 0.8	39.6 ± 1.2
75	2	27.6 ± 1.6	31.9 ± 1.6	28.9 ± 1.4	37.9 ± 1.9	1.8 ± 29.0	37.8 ± 1.9	28.9 ± 1.4	37.9 ± 1.8
75	3	15.5 ± 0.7	20.0 ± 0.7	16.6 ± 0.6	66.0 ± 2.3	2.3 ± 16.6	65.9 ± 2.3	16.6 ± 0.6	66.0 ± 2.3
75	4	28.3 ± 1.1	29.3 ± 0.9	29.4 ± 1.1	37.3 ± 1.3	1.3 ± 29.3	37.3 ± 1.3	29.3 ± 1.1	37.3 ± 1.3
75	5	6.7 ± 0.7	8.8 ± 0.8	7.5 ± 0.6	147.2 ± 12.5	12.5 ± 7.5	147.6 ± 12.4	7.5 ± 0.6	147.6 ± 12.5
75	6	5.6 ± 0.3	6.8 ± 0.4	6.6 ± 0.3	165.1 ± 6.4	6.5 ± 6.6	165.1 ± 6.5	6.6 ± 0.3	165.3 ± 6.5
75	8	4.4 ± 0.5	5.0 ± 0.5	5.6 ± 0.4	196.1 ± 14.2	13.8 ± 5.6	195.9 ± 14.2	5.6 ± 0.4	195.8 ± 13.8

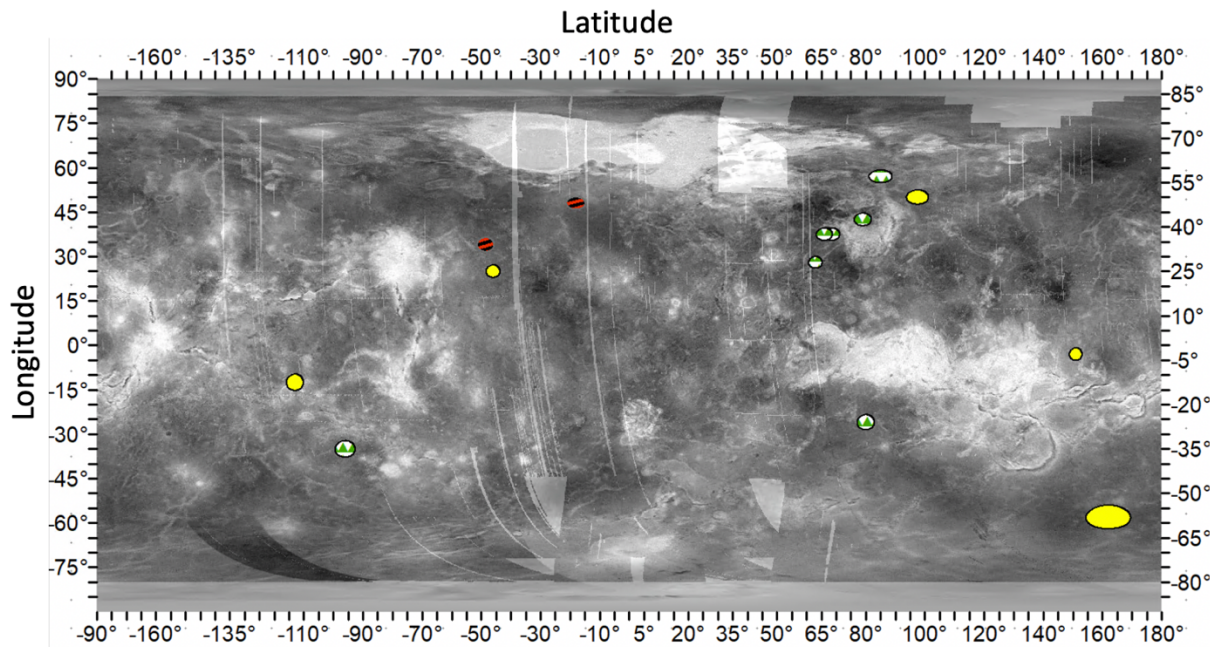


**Figure S1.** Our derived estimates for elastic thickness generally agree with those derived from admittance data (Anderson & Smrekar, 2006). Ellipses representing domes for which we derived elastic thickness overlay a map of global topography. The ellipses are color and pattern coded based on the agreement between our derived elastic thicknesses and those from a global map constructed from admittance (the ratio of gravity to topography). The size of each ellipse represents the resolution of gravity data at that point. Green triangles, solid yellow, and red striped ovals indicate domes with excellent ( $>50\%$  within  $\pm 20$  km), good ( $>0-50\%$ ), and no ( $0\%$ ) agreement, respectively.

**Data Set S1.** Radar images showing the orientation of all topographic profiles around each dome that were drawn using JMARS. The #1 profile points directly north, and the index numbers increase clockwise as labeled in Figure 2.

**Data Set S2.** Raw data (elevation versus distance along track) that was extracted from each topographic profile that was amenable to a flexural interpretation. These data were fit to the equations listed in the main text using the curve-fitting algorithm that is included with Matlab.